On Regularizing the Strongly Nonlinear Internal Wave Model

Tae-Chang Jo
Department of Mathematics
Inha University, Korea

Wooyoung Choi
Dept. of Mathematical Sciences
New Jersey Institute of Technology

CAMS Report 0607-28, Fall 2006/Spring 2007

Center for Applied Mathematics and Statistics

On Regularizing the Strongly Nonlinear Internal Wave Model

Tae-Chang Jo

Department of Mathematics
Inha University
Incheon, Korea

and

Wooyoung Choi

Department of Mathematical Science
New Jersey Institute of Technology
Newark, NJ 07102-1982

Abstract

A strongly nonlinear asymptotic model describing the evolution of large amplitude internal waves in a two-layer system is studied numerically. While the steady model has been demonstrated to capture correctly the characteristics of large amplitude internal solitary waves, a local stability analysis shows that the time-dependent inviscid model suffers from the Kelvin-Helmholtz instability due to a tangential velocity discontinuity across the interface accompanied by the interfacial deformation. An attempt to represent the viscous effect that is missing in the model is made with eddy viscosity, but this simple *ad-hoc* model is shown to fail to suppress unstable short waves. Alternatively, when a smooth low-pass Fourier filter is applied, it is found that a large amplitude internal solitary wave propagates stably without change of form, and mass and energy are conserved well. The head-on collision of two counter-propagating solitary waves is studied using the filtered strongly nonlinear model and its numerical solution is compared with the weakly nonlinear asymptotic solution.

1 Introduction

An increasing number of large amplitude internal solitary waves typically generated by the interaction of stratified tidal flow with strong topographic features have been observed in recent field experiments. The amplitudes of the internal solitary waves measured during this field campaign often exceed 100 meters [1]. The generation and evolution of such large amplitude internal waves are ultimately governed by the Navier-Stokes (NS) equations. However, fully resolved NS simulations are often impractical, in particular, in three-dimensional settings and various asymptotic models have therefore been developed, each relying on an assumption regarding the relative importance of the nonlinear and dispersive terms in the asymptotic expansion procedure. The Korteweg-de Vries (KdV) equation originally derived by Benjamin [2] and Benney [3], for example, assumes that the waves are weakly nonlinear and weakly dispersive. In other words, the wave amplitude is much smaller than, for example, the upper layer thickness and the water depth is much smaller than the typical wavelength. Other theoretical models are discussed in the recent reviews by Ostrovsky & Stepayants [4] and Helfrich & Melville [5].

Although a number of attempts have been made to improve the KdV-type models, the wave amplitudes observed in field experiments are of the same order of magnitude as the upper layer thickness and the domain of validity of these weakly nonlinear models remains limited. To develop a theory that is applicable in the

large amplitude regime, the strongly nonlinear models have been developed by Choi & Camassa [6, 7] for a two-layer system, by assuming that the thickness of one of the two layers is at least much smaller than the characteristic wavelength but imposing no assumption on the wave amplitude, for both shallow and deep configurations where the thickness of the lower layer is comparable to and much greater than that of the upper layer, respectively. For the shallow configuration, the model was found to be identical to that derived earlier by Miyata [8]. These asymptotic models have been shown to be applicable over a wide range of wave amplitudes and layer thicknesses when compared with laboratory experiments and numerical solutions of the Euler equations for large (even near maximum) amplitude internal solitary waves (Ostrovsky & Grue [9]; Camassa *et al.* [10]).

Limitations to the application of the strongly nonlinear models also do exist when an attempt to solve numerically the time-dependent model for the shallow configuration is made. Since it was derived under the inviscid assumption with which only continuity of the normal velocity across the interface is imposed, the model allows a jump in tangential velocity and suffers from the Kelvin-Helmholtz (KH) instability. By assuming that the velocity discontinuity induced by an internal solitary wave appears to be locally uniform at least to short wavelength disturbances that are most unstable in the KH instability, Jo & Choi [11] carried out a local stability analysis and showed that the short-wavelength instability in their numerical simulations is consistent with their stability analysis. It needs to be stressed that this KH instability of an internal solitary wave has been observed when solving not only the strongly nonlinear model, but also the full Euler equations [12]. While density stratification has a stabilizing effect, the shear instability due to the tangential velocity discontinuity is too strong and leads to the growth of short-wavelength disturbances. The initial-value problem with a tangential velocity jump in a two-layer system is therefore ill-posed [13] as the vortex sheet problem in a homogeneous fluid [14], and the strongly nonlinear internal wave model has to be regularized before it is solved numerically. On the other hand, for the deep configuration where the lower layer is much deeper and, therefore, less active, the strongly nonlinear model solves only the upper layer velocity and no KH instability appears.

Although all short wavelength disturbances whose wave numbers are greater than a critical value grow exponentially in time when the shallow configuration model is solved numerically, finite amplitude solitary waves generated in the previous laboratory experiments are found to be stable unless the wave amplitude is very close to the maximum wave amplitude. For example, in the experiment of Grue *et al.* [15], a solitary wave whose amplitude a is 79% of the maximum wave amplitude $a_{\max}$ were shown to propagate without any sign of instability although the Kelvin-Helmholtz billows were observed for a solitary wave of $a/a_{\max} = 0.96$. This discrepancy between the model and the laboratory experiment could be explained by the fact that this *inviscid* model fails to describe the viscous effect inside the boundary layer at the interface that plays an important role in keeping unstable short waves from growing in the laboratory experiment. While it is ideal to develop the viscous model using an asymptotic expansion technique similar to the inviscid strongly nonlinear long wave theory, it is not a trivial task. As a first step toward solving the time-dependent strongly nonlinear internal model, we adopt two simple approaches of an eddy viscosity model and a numerical filter, and test if either approach suppresses this undesirable (often unrealistic for intermediate wave amplitudes) short wave instability without affecting the long wave behavior that the model describes correctly.

While stabilizing short waves in a system of two immiscible fluids, the surface tension that is absent in the interior of the ocean is neglected in this paper. A two-layer system becomes also less unstable as the density difference between the two layers increases, but we assume that the density difference is small for realistic oceanic applications.

2 Mathematical Model and Instability of Solitary Waves

2.1 The strongly nonlinear model

In a two-layer system shown in figure 2.1, when the wavelength λ is long compared to one of the fluid layer thicknesses h_i (with $i = 1$ and 2 representing the upper and lower layers, respectively), it has been shown that strongly nonlinear long wave models for large amplitude internal waves can be obtained using an asymptotic expansion in a small long wave parameter $\epsilon = \lambda/h_i$ without making any assumption on the wave amplitude [7]. In particular, for the shallow configuration where the thicknesses of both layers are small compared

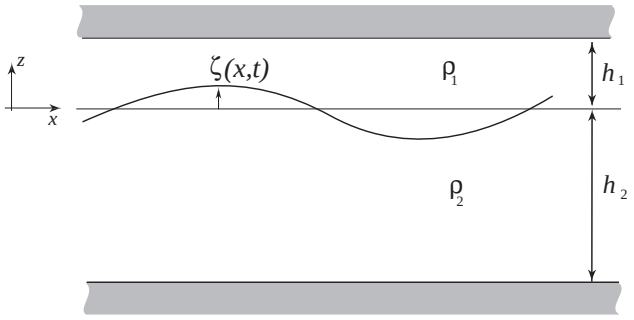

Figure 2.1: The two-fluid system set-up.

to the typical wavelengths, the model can be written, in terms of the displacement of the interface ζ, the depth-averaged velocities u_i, and the pressure at the interface P, as

$$\eta_{it} + (\eta_i u_i)_x = 0\,, \tag{2.1}$$

$$u_{it} + u_i u_{ix} + g\zeta_x = -\frac{P_x}{\rho_i} + \frac{1}{\eta_i}\left(\frac{1}{3}{\eta_i}^3 G_i\right)_x\,, \tag{2.2}$$

where g is the gravitational acceleration, ρ_i is the fluid density with $\rho_1 < \rho_2$ for a stable stratification, and the subscripts x and t represent partial differentiation with respect to space and time, respectively. The layer thickness η_i and the depth-averaged velocity u_i are defined by

$$\eta_1(x,t) = h_1 - \zeta(x,t)\;, \quad u_1(x,t) = \frac{1}{\eta_1}\int_{\zeta}^{h_1} U_1(x,z,t)\,\mathrm{d}z\,, \tag{2.3}$$

$$\eta_2(x,t) = h_2 + \zeta(x,t), \qquad u_2(x,t) = \frac{1}{\eta_2}\int_{-h_2}^{\zeta} U_2(x,z,t)\,\mathrm{d}z\,, \tag{2.4}$$

where $U_i(x,z,t)$ is the horizontal fluid velocity. Notice that the model contains the nonlinear dispersive effect denoted by G_i:

$$G_i(x,t) = u_{ixt} + u_i u_{ixx} - (u_{ix})^2\,, \tag{2.5}$$

which comes from the non-hydrostatic pressure contribution with an error of $O(\epsilon^4)$.

After eliminating P_x from (2.2) for $i = 1$ and 2 and using the relationship between u_1 and u_2 found from (2.1):

$$u_2 = -\left(\frac{\eta_1}{\eta_2}\right) u_1\,, \tag{2.6}$$

the system of equations (2.1)–(2.2) can be further reduced to a closed system of two evolution equations for η_1 and u_1 (or u_2).

2.2 Solitary waves and their stability

For a solitary wave of speed c, the strongly nonlinear model (2.1)–(2.2) becomes, in a frame of reference moving with the solitary wave ($X = x - ct$) [7, 16]

$${\zeta_X}^2 = \frac{3\zeta^2\Big[\rho_1 c^2\eta_2 + \rho_2 c^2\eta_1 - g(\rho_2-\rho_1)\eta_1\eta_2\Big]}{\rho_1 c^2 {h_1}^2\eta_2 + \rho_2 c^2 {h_2}^2\eta_1}\,. \tag{2.7}$$

The solitary wave can be of elevation for $(h_2/h_1) < (\rho_2/\rho_1)^{1/2}$ and of depression for $(h_2/h_1) > (\rho_2/\rho_1)^{1/2}$, while no solitary wave solution exists at the critical depth ratio given by $(h_2/h_1) = (\rho_2/\rho_1)^{1/2}$. The solitary wave speed c can be written, in terms of wave amplitude a, as

$$\frac{c^2}{c_0^2} = \frac{(h_1-a)(h_2+a)}{h_1h_2 - (c_0^2/g)a}, \qquad {c_0}^2 = \frac{gh_1h_2(\rho_2-\rho_1)}{\rho_1h_2+\rho_2h_1}\,, \tag{2.8}$$

with the maximum wave amplitude and wave speed given by

$$a_m = \frac{h_1 - h_2\sqrt{\rho_1/\rho_2}}{1+\sqrt{\rho_1/\rho_2}}\,, \qquad {c_m}^2 = g(h_1+h_2)\frac{1-\sqrt{\rho_1/\rho_2}}{1+\sqrt{\rho_1/\rho_2}}\,, \tag{2.9}$$

beyond which no solitary wave solution exists.

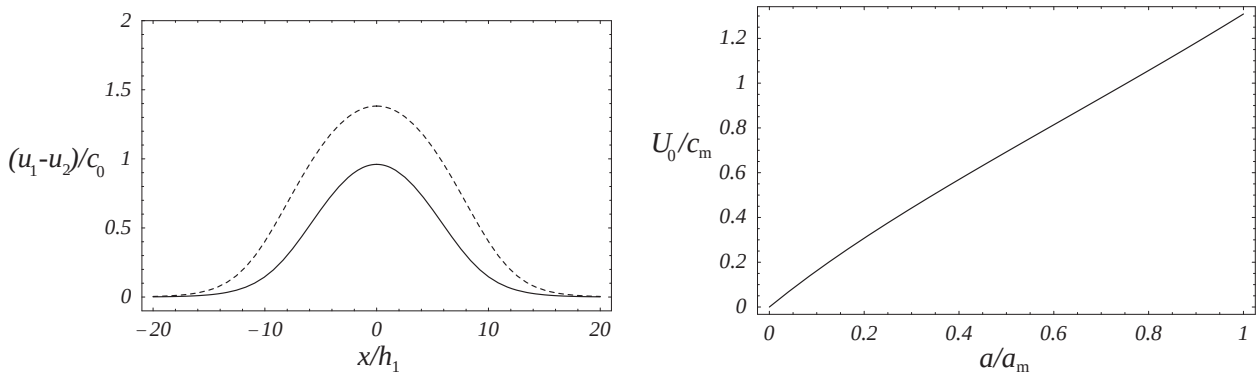

Figure 2.2: (a) The velocity jump $u_1(x) - u_2(x)$ induced by a solitary wave of $a/h_1 = -1$ (—-) and -1.5 (- - -) for $\rho_2/\rho_1 = 1.003$ and $h_2/h_1 = 4.8$. (b) The velocity jump at the wave crest versus wave amplitude, where a_m/h_1=-1.8978 and $c_m/\sqrt{gh_1}$=0.0659.

Despite excellent agreement with laboratory experiments for a wide range of wave amplitudes [10], the solitary wave solution of this *inviscid* model is accompanied by an undesirable tangential velocity discontinuity across the interface, which in turn introduces a jump in the horizontal velocity given, from (2.1) for $i = 1, 2$, by

$$u_1 - u_2 = -c\,\zeta\left(\frac{1}{h_1-\zeta} + \frac{1}{h_2+\zeta}\right)\,, \tag{2.10}$$

where c is positive for the right-going waves. From figure 2.2(a), it can be seen that the horizontal velocity jump becomes maximum at the location of maximum interfacial displacement

$$U_0 \equiv (u_1 - u_2)_{\text{at } x=0} = -\frac{ca(h_1+h_2)}{(h_1-a)(h_2+a)}, \tag{2.11}$$

and vanishes as $|x|$ approaches to infinity. The maximum velocity jump U_0 increases as the wave amplitude increases, as shown in figure 2.2(b). Notice that the velocity jump occurs for any non-zero value of a, implying that the time-dependent model initialized with a deformed interface can suffer from the Kelvin-Helmholtz instability when it is solved numerically.

Since the horizontal velocity u_i induced by an internal solitary wave varies slowly in x, the velocity jump can be assumed to be locally uniform in space, in particular, near the wave crest where the maximum velocity jump occurs and one can perform a local stability analysis to find the following criterion for instability [11]:

$${U_0}^2 > \frac{g(\rho_2-\rho_1)(\rho_1\alpha_1 h_2 + \rho_2\alpha_2 h_1)}{\rho_1\rho_2\alpha_1\alpha_2}, \tag{2.12}$$

where

$$\alpha_i = 1 + \tfrac{1}{3}k^2{h_i}^2. \tag{2.13}$$

For long waves of small kh_i, as shown in figure 2.3(a), the stability criterion (2.12) from the long wave model compares well with the full linear theory given by

$${U_0}^2 > \frac{g(\rho_2-\rho_1)}{k}\left[\frac{\tanh(kh_1)}{\rho_1} + \frac{\tanh(kh_2)}{\rho_2}\right], \tag{2.14}$$

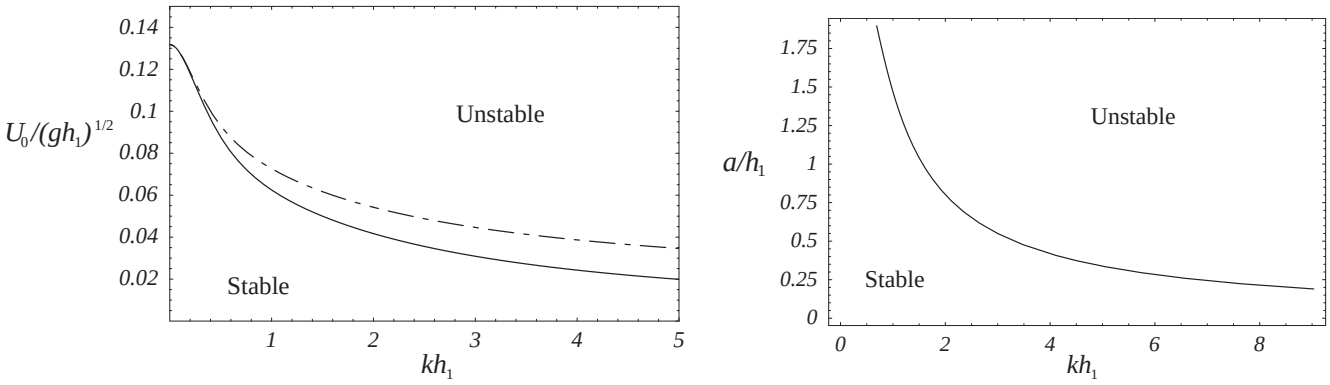

Figure 2.3: (a) Neutral stability curve for U_0 versus k: ——, inviscid long wave theory given by (2.12); — - —, inviscid full linear theory given by (2.14). (b) Neutral stability curve for a versus k from the long wave model.

although the long wave model with a fixed value of U_0 becomes unstable for a smaller value of k than what the full linear theory predicts, as shown in figure 2.3(a).

Since the maximum velocity jump across the interface U_0 given by (2.11) depends on wave amplitude for fixed density and depth ratios, (2.12) determines the critical wave number ($k_{\rm crit}$), as a function of wave amplitude a, beyond which all short-wave disturbances grow exponentially in time. When computing the critical wave number shown in figure 2.3(b), the undisturbed layer thickness h_1 and h_2 in (2.12) are replaced, for large amplitude effects to be taken into consideration, by the local thicknesses of the upper and lower layers defined by

$$\bar{h}_1 = h_1 - a, \qquad \bar{h}_2 = h_2 + a. \tag{2.15}$$

Although the stability criterion given by (2.12) is based on a local stability analysis by assuming that the solitary wave profile changes little over the length scales of small disturbances (and so does the velocity jump), it has been found consistent with the time-dependent numerical simulations for the propagation of a single solitary wave [11].

2.3 Eddy viscosity model

The viscous effect could be a crucial physical mechanism to lessen the Kelvin-Helmholtz-type instability, but it is beyond the scope of this paper to incorporate the viscous effect in a systematic way into the strongly nonlinear model. Instead, we briefly investigate a simple but *ad-hoc* eddy viscosity model that is often adopted in the long wave models. As mentioned previously, while it plays an important role in the interfacial dynamics between two immiscible fluids, the surface tension is irrelevant in the dynamics of internal solitary waves in the ocean and will not be considered here.

An eddy viscosity term D_i parameterized as

$$D_i = \frac{1}{\rho_i \eta_i}\Big(\mu_e \eta_i u_{ix}\Big)_x, \tag{2.16}$$

is added to the momentum equation:

$$u_{it} + u_i u_{ix} + g\zeta_x = -\frac{P_x}{\rho_i} + \frac{1}{\eta_i}\left(\frac{1}{3}{\eta_i}^3 G_i\right)_x + D_i\,, \tag{2.17}$$

where μ_e is the eddy viscosity. From (2.17), it can be shown that the total energy E defined by

$$E = \int \tfrac{1}{2}(\rho_2 - \rho_1) g\zeta^2 \,\mathrm{d}x + \sum_{i=1}^{2} \rho_i \int \tfrac{1}{2}\left(\eta_i\, {u_i}^2 + \tfrac{1}{3}{\eta_i}^3 {u_{ix}}^2\right)\mathrm{d}x, \tag{2.18}$$

is no longer a conserved quantity and its time rate of change is given by

$$\frac{\mathrm{d}E}{\mathrm{d}t} = \sum_{i=1}^{2} \int \rho_i \eta_i u_i \, D_i \, \mathrm{d}x = -\sum_{i=1}^{2} \int \mu_e \, \eta_i {u_{ix}}^2 \mathrm{d}x \; < 0. \tag{2.19}$$

When linearized about constant states for u_i, equations (2.1) and (2.17) with assuming solutions in the form of $\mathrm{e}^{\mathrm{i}(kx-\omega t)}$ yield the following equation from which the linear dispersion relation between wave frequency ω and wave number k can be found:

$$A\omega^2 - 2B\omega + C = 0, \tag{2.20}$$

where A, B, and C are given by

$$A = \rho_1 h_2 \alpha_1 + \rho_2 h_1 \alpha_2, \quad B = \rho_1 h_2 k \alpha_1 u_1 + \rho_2 h_1 k \alpha_2 u_2 - \mathrm{i}\mu_e (h_1 + h_2) k^2/2 \equiv B_R + \mathrm{i}B_I, \tag{2.21}$$

$$C = \rho_1 h_2 k^2 \alpha_1 u_1^2 + \rho_2 h_1 k^2 \alpha_2 u_2^2 - g h_1 h_2 (\rho_2 - \rho_1) k^2 - \mathrm{i}\mu_e (h_2 u_1 + h_1 u_2) k^3 \equiv C_R + \mathrm{i}C_I. \tag{2.22}$$

For $\mu_e = 0$, the linear stability criterion given by (2.12) can be recovered and it can be shown that the solution of (2.20) for ω with $\mu_e = 0$ is the long wave limit of the full linear dispersion relation which can be obtained from (2.20) by replacing A, B, and C by

$$A = \rho_1 \coth(kh_1) + \rho_2 \coth(kh_2), \quad B = k\Big[\rho_1 U_1 \coth(kh_1) + \rho_2 U_2 \coth(kh_2)\Big], \tag{2.23}$$

$$C = k^2\Big[\rho_1 {U_1}^2 \coth(kh_1) + \rho_2 {U_2}^2 \coth(kh_2)\Big] - (\rho_2 - \rho_1) g k. \tag{2.24}$$

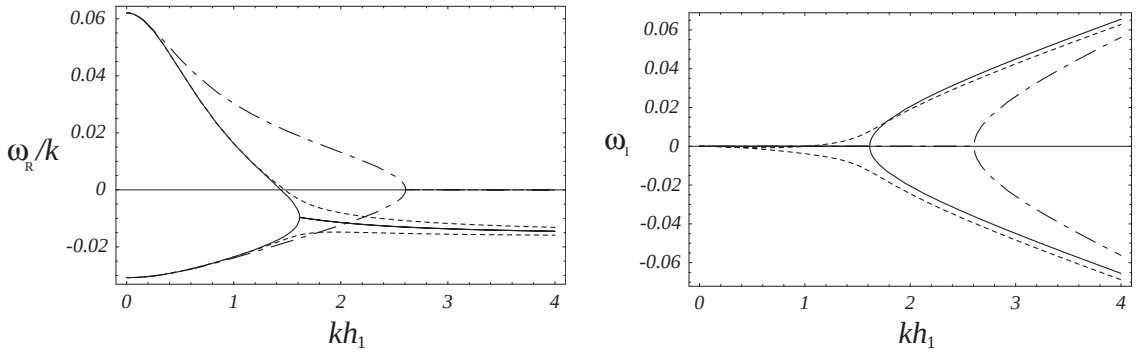

Figure 2.4: Real and imaginary parts of ω for $U_0/\sqrt{gh_1} \simeq 0.0478$ which corresponds to a velocity jump induced by a solitary wave of wave amplitude $a = -1$: ——, inviscid long wave theory; — - —, inviscid full linear theory; - - - -, 'viscous' long wave model with $\mu_e = 0.01$. (a) Wave speed (ω_R/k) versus k. (b) ω_I versus k. A positive imaginary part represents the growth rate.

In figure 2.4, the real and imaginary parts of ω from the viscous long wave model with $\mu_e = 0.01$ are compared with those from the inviscid long wave model and the full linear theory. For small k, the real part of ω or the linear wave speed defined by ω_R/k from both the viscous and inviscid long wave models agree well with that from the inviscid full linear theory while the discrepancy between the long wave models and the full linear theory increases as k increases. In both the inviscid long wave model and the full linear theory, the two neutrally stable modes collide at the critical wave numbers (k_{crit}) beyond which a non-vanishing positive imaginary part of ω (equivalently, the growth rate) appears. Large amplitude internal solitary waves are therefore expected to be unstable to disturbances of wavenumber k_{crit} or higher although the values of k_{crit} are different in the two inviscid approaches. For $\mu_e \neq 0$, the viscous long wave model has a branch whose positive imaginary part appears at a wavenumber that is smaller than k_{crit} although the absolute value of the imaginary part is smaller. This implies that the eddy viscosity term in (2.17) destabilizes a neutrally stable inviscid mode for k smaller than k_{crit}. A bi-Laplacian dissipative term given by $D_i = -(\mu_e \eta_i u_{ixx})_{xx}/(\rho_i \eta_i)$ with a small value of μ_e is also considered, but it does not stabilize the system. Thus, it can be concluded that neither Laplacian nor bi-Laplacian dissipative term is an appropriate model to represent the physical viscous effect on internal wave dynamics.

a	-0.1	-0.5	-1.0	-1.2	-1.4	-1.6	-1.8	-1.85	-1.89
$k_{\rm crit}$	17.3	3.32	1.59	1.28	1.06	0.895	0.753	0.721	0.695
$\Delta x_{\rm crit}$	0.182	0.946	1.976	2.454	2.964	3.510	4.172	4.357	4.520

Table 3.1: Critical wavenumber ($k_{\rm crit}$) for a solitary wave of amplitude a and the corresponding critical grid space ($\Delta x_{\rm crit}$). Any disturbances whose wave numbers are greater than $k_{\rm crit}$ become unstable. Equivalently, numerical computations with a grid space smaller than $\Delta x_{\rm crit}$ are expected to be unstable.

3 Numerical Results with a Low-pass Filter

In our numerical computations, as in Jo & Choi [11], we first reduce (2.1)–(2.2) for $i = 1, 2$ to a system of coupled equations for ζ and u_1 by subtracting (2.2) for $i = 1, 2$ to eliminate P and using (2.6) to express u_2 in terms of ζ and u_1. Then, we solve the resulting system using the second-order central difference scheme both in space and in time. For example, for a solitary wave moving to the positive x-direction, we impose the following boundary conditions at the ends of the computational domain: $\zeta = u_1 = 0$ at $x = L$ and the (linear) radiation boundary conditions at $x = -L$, which can be written as $\zeta_t + c_0\zeta_x = 0$ and $u_{1t} + c_0 u_{1x} = 0$, where c_0 is the linear long wave speed given by (2.8). The computational domain is chosen large so that only small amplitude disturbances arrive at the boundary at $x = -L$ where the linear radiation boundary conditions are used. To fix length and time scales, we choose $h_1 = 1$ and $g = 1$ while the length of the computation domain is $2L = 200$. Other physical parameters involved in the results shown here are $\rho_2/\rho_1 = 1.003$ and $h_2 = 4.8$.

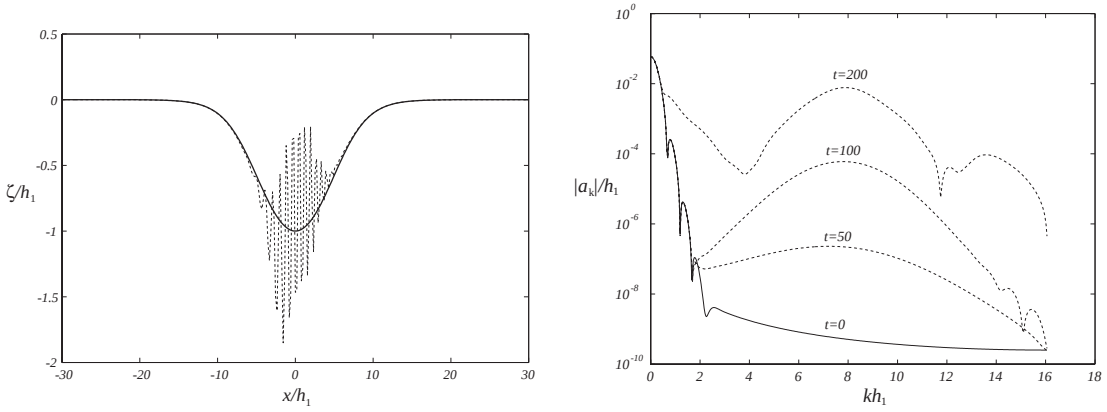

Figure 3.1: Unstable numerical solution (- - -) of a single solitary wave of amplitude $a = -1$. (a) $\zeta(x,t)$ at $t = 150$ compared with the initial condition (—). (b) Evolution of the absolute values of the Fourier coefficients at $t = 0, 50, 100, 150$.

Table 3.1 shows the critical wave number $k_{\rm crit}$ and the corresponding critical grid space defined by $\Delta x_{\rm crit} = 2\pi/(2k_{\rm crit})$ for a few values of wave amplitude up to almost the maximum value of $a_m \simeq -1.8978$. For example, a solitary wave of $a = -1$ whose amplitude is 53% of the maximum amplitude is expected to be linearly unstable for disturbances whose wavenumber is greater than $k_{\rm crit} \simeq 1.59$, or, equivalently, if the grid space is smaller than $\Delta x_{\rm crit} \simeq 1.976$. As shown in figure 3.1$(a)$, instability appears in our numerical computation with a uniform grid space of $\Delta x = 200/1024 \simeq 0.195$ and a fixed time step of $\Delta t = 0.1$. Initially, a perturbation of a wavelength corresponding to the distance between 5 consecutive grid points involved in our central difference scheme of the third-order derivatives in the model grow, as can be seen in figure 3.1(b), but, for large $t > 150$, the higher wavenumber modes grow much faster. The occurrence of instability observed at $t = O(10^2)$ in the present computation can be delayed slightly with a higher-order scheme and a higher precision computation, but cannot be completely removed.

With keeping in mind that the strongly nonlinear model for the shallow configuration captures correctly the long wave behavior, as demonstrated by excellent agreement of the model with numerical solutions of

$a = -1.0$, $k_{f_1} \simeq 1.45$

N_{filter}	20	40	60	80
Δ_M	4.27E-4	3.77E-4	3.43E-4	unstable
Δ_E	2.57E-6	1.29E-6	8.64E-7	unstable

$a = -1.4$, $k_{f_1} \simeq 0.974$

N_{filter}	20	40	50	60
Δ_M	2.70E-4	2.63E-4	2.54E-4	unstable
Δ_E	2.56E-4	1.27E-4	1.02E-4	unstable

$a = -1.8$, $k_{f_1} \simeq 0.691$

N_{filter}	20	30	40	50
Δ_M	1.28E-3	7.99E-4	5.63E-4	unstable
Δ_E	2.37E-3	1.57E-3	1.18E-3	unstable

Table 3.2: Relative errors defined by (3.3) for varying N_{filter} with $k_{f_2} = 2.01$.

the Euler equations and laboratory experiments for internal solitary waves, it could be justified to adopt a numerical filter representing the viscous effect to suppress the short-wave instability without affecting the long-wavelength behavior. Assuming that significant viscous dissipation occurs only in the high wavenumber regime, we adopt the following smooth low-pass filter to keep unstable short-wavelength disturbances from growing:

$$f_k = \begin{cases} 1 & \text{for } k < k_{f_1} \\ \cos^2\left[\frac{\pi(k-k_{f_1})}{2(k_{f_2}-k_{f_1})}\right] & \text{for } k_{f_1} \le k \le k_{f_2} \\ 0 & \text{for } k_{f_2} < k \end{cases}, \tag{3.1}$$

and apply it to the Fourier coefficients of ζ and u_1 every N_{filter} time steps. Then, numerical solutions at $t = 10^4$ (or, equivalently, after a solitary wave has propagated a distance of, approximately, $500h_1$) are presented. A typical choice of k_{f_1} is approximately $0.9k_{\text{crit}}$, where k_{crit} is the critical wavenumber computed in table 3.1, and the cutoff wave number k_{f_2} is chosen to be a constant. To examine validity of the filter given by (3.1), we monitor carefully conservation of mass M and energy E defined by

$$M(t) = \int \zeta \, dx, \qquad E(t) = \int \tfrac{1}{2}(\rho_2 - \rho_1) g \zeta^2 \, \mathrm{d}x + \sum_{i=1}^{2} \rho_i \int \tfrac{1}{2} \left(\eta_i \, {u_i}^2 + \tfrac{1}{3} {\eta_i}^3 {u_{ix}}^2 \right) \mathrm{d}x, \tag{3.2}$$

and measure the maximum relative errors, Δ_M and Δ_E defined by

$$\Delta_M = \max \left| \frac{M(t) - M(0)}{M(0)} \right| \quad , \quad \Delta_E = \max \left| \frac{E(t) - E(0)}{E(0)} \right|. \tag{3.3}$$

To find an optimum filtering frequency, the maximum relative errors in mass and energy conservation are computed for three different wave amplitudes of $a = -1.0$ -1.4, -1.8 with a fixed cutoff wavenumber of $k_{f_2} = 2.01$. As shown in table 3.2, both Δ_M and Δ_E decrease as we apply the filter given by (3.1) less frequently. In other words, more accurate solutions (in terms of conservation of mass and energy) can be obtained as N_{filter} increases, but instability appears if N_{filter} is chosen too large, as expected. It is interesting to notice that mass and energy are conserved relatively well even though only a small number of Fourier modes are kept, in particular, for the case of $a = -1.8$ that is close to the maximum wave amplitude. While the numerical filter is assumed to emulate viscous dissipation and its use can be justified for some range of wave amplitudes for which stable solitary waves are observed in laboratory experiments of Grue *et al.* [15], it still needs to be determined, for example, by physical experiments how large amplitude internal solitary wave can be stabilized by real viscosity.

$a = -1.0$, N_{filter}= 60, $k_{f_1} \simeq 1.45$

k_{f_2}	2.01	4.02	8.04	12.1
Δ_M	3.43E-4	3.19E-4	2.93E-4	unstable
Δ_E	8.64E-7	6.62E-8	4.09E-8	unstable

$a = -1.4$, N_{filter}= 50, $k_{f_1} \simeq 0.974$

k_{f_2}	2.01	4.02	8.02	12.1
Δ_M	2.54E-4	2.48E-4	unstable	unstable
Δ_E	1.02E-4	1.36E-5	unstable	unstable

$a = -1.8$, $N_{\text{filter}} = 30$, $k_{f_1} \simeq 0.691$

k_{f_2}	2.01	4.02	8.02	12.1
Δ_M	7.99E-4	unstable	unstable	unstable
Δ_E	1.57E-3	unstable	unstable	unstable

Table 3.3: Relative errors in conservation of mass and energy defined by (3.3) for different choices of k_{f_2}.

The five-point smoothing formula of Loguet-Higgins & Cokelet [17] has been also tested to suppress the instability observed initially, but conservation of mass and energy is less satisfactory than the filter given by (3.1). For example, when the smoothing formula is used every time step for the solitary wave of $a = -1.0$, Δ_M and Δ_E are found to be 3.33×10^{-3} and 1.54×10^{-2}, respectively, which are much greater than those in table 3.2. While these errors decrease slightly with increasing N_{filter}, the solitary wave profile is then deformed considerably and, therefore, no smoothing formula is considered in this paper.

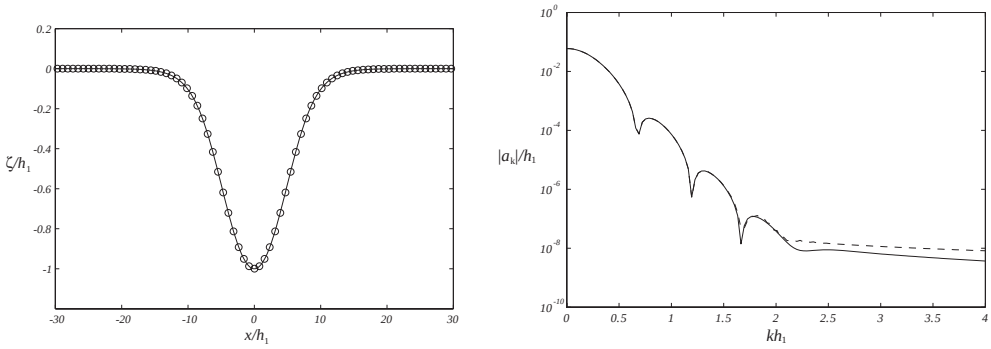

Figure 3.2: Numerical solution of a solitary wave of amplitude $a = -1$: (a) The interfacial displacement, $\zeta(x,t)$ at $t = 10^4$ ($\circ$) compared with the exact solution (—); (b) The absolute value of the Fourier coefficient (- - -) of the numerical solution in (a) compared with that of the exact solution (—).

Next, the relative errors in mass and energy conservation for varying cutoff wavenumber k_{f_2} is examined with fixed N_{filter}. While Δ_M and Δ_E are reduced, increasing k_{f_2} brings more high-wavenumber modes in our computations that are prone to instability. As shown in table 3.3, our numerical solutions with large k_{f_2} become unstable and the choice of k_{f_2} is rather limited, in particular, for large amplitude waves. We can apply the filter more often by decreasing N_{filter}, but the relative errors Δ_M and Δ_E would increase, as demonstrated in table 3.2. For a solitary wave of amplitude $a = -1.8$ (almost 95% of the maximum wave amplitude), a range of admissible k_{f_2} is relatively narrow ($k_{f_2} = 2.01$ or less) and this might imply that real viscosity in physical experiments for large amplitude solitary waves might fail to keep intermediate wavenumber components from growing. Then, unstable local disturbances would grow to develop the Kelvin-Helmholtz billows often observed in laboratory experiments for large amplitude waves.

Numerical solutions for solitary waves of a=-1.0, -1.4, -1.8 at $t = 10^4$ with cutoff wavenumber $k_{f_2} = 2.01$ are shown in figures 3.2–3.4 with $N_{\text{filter}} = 60$, 50, 30, respectively. When compared with the initial conditions

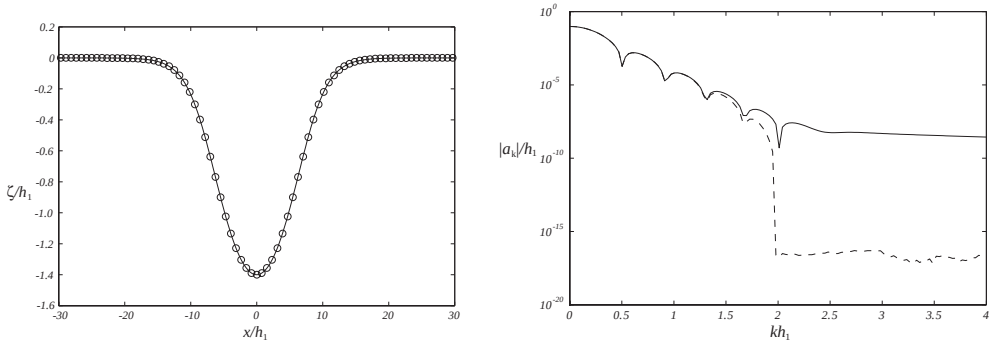

Figure 3.3: (a) Numerical solution of a solitary wave of amplitude $a = -1.4$: (a) The interfacial displacement, $\zeta(x,t)$ at $t = 10^4$ ($\circ$) compared with the exact solution (—); (b) The absolute value of the Fourier coefficient (- - -) of the numerical solution in (a) compared with that of the exact solution (—).

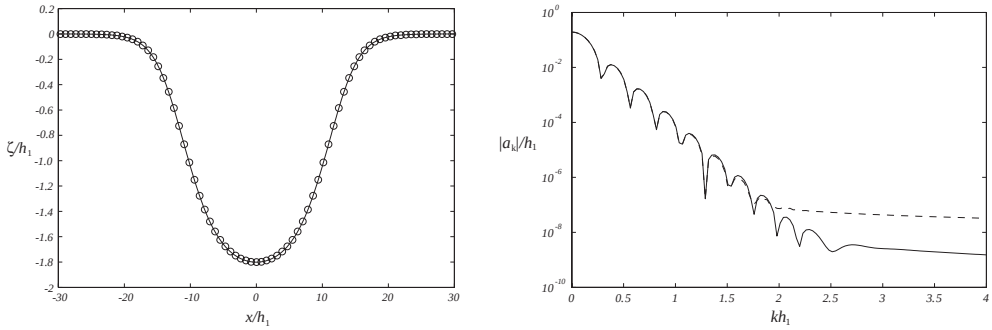

Figure 3.4: (a) Numerical solution of a solitary wave of amplitude $a = -1.8$: (a) The interfacial displacement, $\zeta(x,t)$ at $t = 10^4$ ($\circ$) compared with the exact solution (—); (b) The absolute value of the Fourier coefficient (- - -) of the numerical solution in (a) compared with that of the exact solution (—).

(that are also the exact solutions in a frame of reference moving with the solitary waves), the numerical solutions show excellent agreement. The Fourier coefficients in figures 3.2–3.4 (log-linear plots) clearly indicate that the filter suppresses the growth of unstable high-wavenumber disturbances, but leave intact the low-wavenumber modes that the strongly nonlinear model captures correctly. Notice that the magnitudes of the Fourier coefficients for large k at $t = 10^4$ in figures 3.2–3.4 vary since we use different filtering frequencies for different wave amplitudes.

4 Head-on Collision

To test the filter given by (3.1) for a time-dependent problem, we consider the head-on collision of two counter-propagating solitary waves of large amplitudes and the higher-order nonlinear effects on the collision process is examined. Figure 4.1 shows the head-on collision of two identical solitary waves of a=-1 and numerical solutions at $t = 0$, 400, 680, and 1400 are compared with the linear superposition of the two solitary waves counter-propagating with their own wave speeds. Before they collide, little interaction between the two waves occurs. During the collision, they merge into a single peak whose height is slightly higher than a linear sum of the two wave heights. After collision, they almost recover their original shape except for much shorter linear dispersive tails along with a small phase shift. These trailing small dispersive tails are also observed in the head-on collision of finite amplitude surface solitary waves [18]. In order to quantify the higher-order nonlinear effects, the peak wave height (or runup) during the symmetric head-on collision and the phase shift after the collision are measured and compared with the weakly nonlinear asymptotic results,

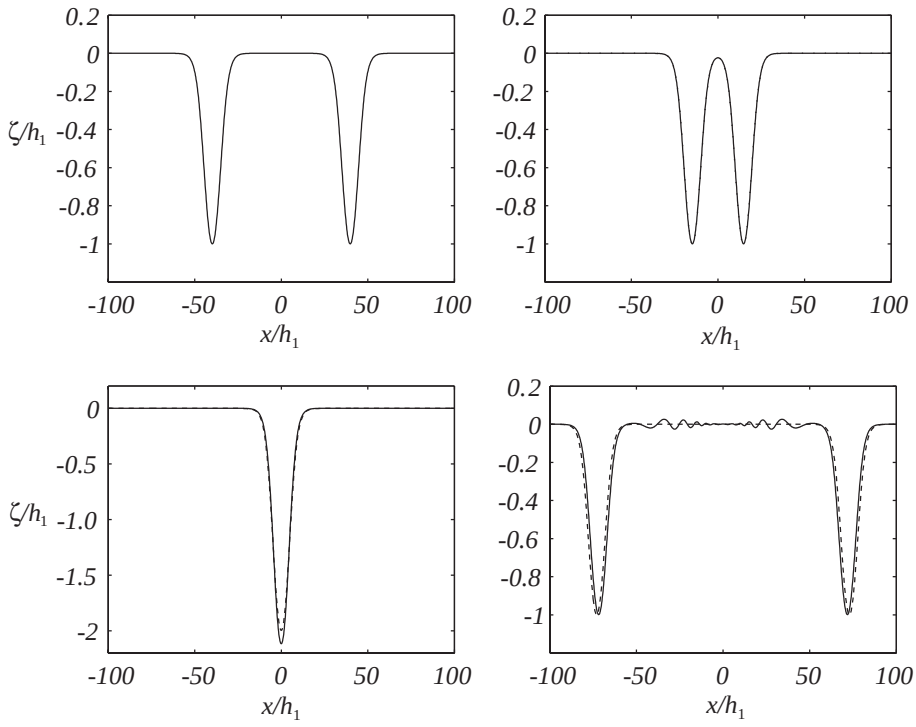

Figure 4.1: Symmetric head-on collision of two counter-propagating solitary waves of $a = -1.0$ at t=0, 400, 640, and 1800: Numerical solutions (—) compared with the linear superposition of the two solitary waves (– – –)

for example, in [11]:

$$\Delta\zeta = \alpha a^2, \qquad \Delta x_p = \gamma |a|^{1/2}, \tag{4.1}$$

where a is the wave height of the solitary wave, $\Delta\zeta$ (negative for depression waves) measures the deviation of the peak height from $2a$, Δx_p is the phase shift, $\alpha \simeq -0.396$, and $\gamma \simeq 1.126$.

As shown in figure 4.2, for smaller wave amplitudes, approximately, up to $|a|/h_1 \simeq 0.3$, the deviation of the peak height ($\Delta\zeta$) from a linear sum of two wave heights ($2a$) increases with the wave amplitude at a rate predicted by (4.1). For larger wave amplitudes, $\Delta\zeta$ increases at a much slower rate with the wave amplitude and even decreases approximately beyond $|a|/h_1 \simeq 1$. On the other hand, the phase shift (Δx) from numerical simulations of the strongly nonlinear model matches well with the weakly nonlinear prediction given by (4.1).

5 Discussion

To describe the evolution of large amplitude internal long waves in an inviscid two-layer system, we have studied the strongly nonlinear model for the shallow configuration obtained by Miyata [8] and Choi & Camassa [7]. Although it has been shown that the strongly nonlinear model captures correctly the essential characteristics of large amplitude internal solitary waves [10], the short-wave instability excited by a velocity jump across the interface causes a difficulty in solving the time-dependent model numerically. While it has a stabilizing effect, a density jump in the ocean is often too small to overcome the Kelvin-Helmholtz instability. Two different approaches are taken to regularize the strongly nonlinear model in this paper: eddy viscosity and numerical filter. A simple eddy viscosity model is found to fail to regularize the problem, but it is shown that a low-pass smooth filter suppresses unstable high wavenumber modes and the evolution of large amplitude internal waves can be successfully simulated. Furthermore, physical conservation laws are kept

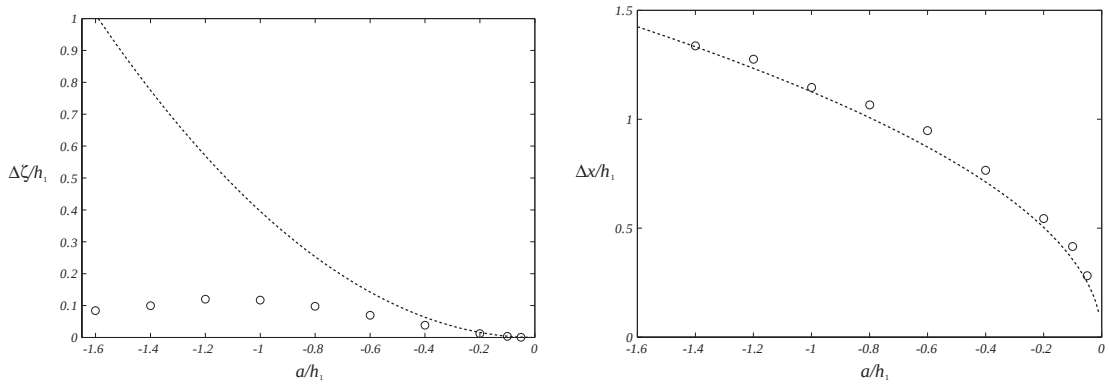

Figure 4.2: Deviation of the peak height from $2a$ during the head-on collision: numerical solutions (o) and weakly nonlinear result (—) given by (4.1).

well with an error much less than 1%, implying that the filter has little impact on low wavenumber modes that are important in the dynamics of internal solitary waves.

A simple eddy viscosity model with either Laplacian or bi-Laplacian dissipative terms is found to be unable to represent the real viscous effect and it would be of interest to develop a systematic viscous model in the future to describe the evolution of large amplitude internal waves in the small-viscosity limit. Since the viscous effect on the shear instability in a two-layer system would appear mostly inside the boundary layer at the interface, the viscous velocity profile that is continuous across the interface might be obtained by solving the boundary layer equations. Then, a local stability analysis can be carried out to better understand stability characteristics of large amplitude internal solitary waves under the viscous effect and is expected to provide a clue to how to parameterize its effect into the asymptotic model. To validate such a viscous model, it would be required to carry out direct numerical simulations of the Navier-Stokes equations with resolving thin boundary layers at the interface.

Continuous density stratification is another physical effect present in laboratory experiments with miscible fluids but missing in the two-layer model. For a continuous stratified fluid, although no velocity jump occurs inside the fluid domain even under the inviscid assumption, the velocity profile varies rapidly in depth inside a thin pycnocline, leading to a large velocity gradient that increases with wave amplitude. For a finite amplitude solitary wave, the Richardson number inversely proportional to the square of the velocity gradient could be smaller than a critical value of 0.25 [19] and the solitary wave in the absence of viscosity is still theoretically unstable. Therefore, the viscous effect still plays a role for the case of continuous stratification and needs to be modeled appropriately.

Acknowledgement

The work of WC is supported by the National Science Foundation through Grant DMS-0620832 and TC is supported by the Inha University through Research Grant INHA-33920.

References

[1] S. R. Ramp, D. Tang, T. F. Duda, J. F. Lynch, A. K. Liu, C. S. Chiu, F. Bahr, H. R. Kim, and Y. J. Yang, Internal solitons in the Northeastern South China Sea. Part I: Sources and deep water propagation. *IEEE J. Ocean Engineering* 29:1157–1181 (2004).

[2] T. B. Benjamin, Internal waves of finite amplitude and permanent form. *J. Fluid Mech.* 25:241–270 (1966).

[3] D. J. Benney, Long nonlinear waves in fluid flows. *J. of Math. Phys.* 45:52.–69 (1966).

[4] L. A. Ostrovsky and Y. A. Stepanyants, Internal solitons in laboratory experiments: Comparison with theoretical models. *Chaos* 15:037111-1:28 (2005).

[5] K. R. Helfrich and W. K. Melville, Long nonlinear internal waves. *Ann. Rev. Fluid Mech.* 38:395–425 (2006).

[6] W. Choi and R. Camassa, Long internal waves of finite amplitude. *Phys. Rev. Lett.* 77:1759–1762 (1996).

[7] W. Choi and R. Camassa, Fully nonlinear internal waves in a two-fluid system, *J. Fluid Mech.* 396:1–36 (1999).

[8] M. Miyata, Long internal waves of large amplitude. *Proc. IUTAM Symp. on Nonlinear Water Waves*, Horikawa, H. and Maruo, H. (eds), 399–406 (1988).

[9] L. A. Ostrovsky and J. Grue, Evolution equations for strongly nonlinear internal waves. *Phys. Fluids* 15:2934–2948 (2003)

[10] R. Camassa, W. Choi, H. Michallet, P. Rusas, and J. K. Sveen, On the realm of validity of strongly nonlinear asymptotic approximations for internal waves. *J. Fluid Mech.* 549:1-23 (2006).

[11] T.-C. Jo and W. Choi, Dynamics of strongly nonlinear solitary waves in shallow water, *Stud. Appl. Math.* 109:205–227 (2002).

[12] J. Grue, H.A. Friss, E. Palm and P. O. Rusas, A method for computing unsteady fully nonlinear interfacial waves. *J. Fluid Mech.* 351:223–252 (1997).

[13] R. Liska, L. Margolin, and B. Wendroff, Nonhydrostatic two-layer models of incompressible flow. *Computers Math. Applic.* 29:25–37 (1995).

[14] R. Krasny Desingularization of Periodic Vortex Sheet Roll-up. *J. of Comp. Phys.* 65:292–313 (1986).

[15] J. Grue, A. Jensen, P. E. Rusas, and J. K. Sveen, Properties of large amplitude internal waves. *J. Fluid Mech.* 380:257–278 (1999).

[16] M. Miyata, An internal solitary wave of large amplitude. *La mer* 23:43–48 (1985).

[17] M. Longuet-Higgins and E. Cokelet, The deformation of steep surface waves in water. I. A numerical method of computation. *Proc. of the R. Soc. of Lond. A* 350:1–26 (1976).

[18] Y. A. Li, J. M. Hyman, and W. Choi, A numerical study of the exact evolution equations for surface waves in water of finite depth. *Studies in Applied. Math.* 113:303–324 (2004).

[19] P. G. Drazin and W. H. Reid, *Hydrodynamic Stability*, Cambridge (1981).